

# Continuous fibre composite 3D printing with pultruded carbon/PA6 commingled fibres: processing and mechanical properties\*

Peng Zhuo<sup>a,\*</sup>, Shuguang Li<sup>b,\*\*</sup>, Ian A. Ashcroft<sup>b</sup> and Arthur I. Jones<sup>b</sup>

<sup>a</sup>AVIC Composite Technology Centre, Beijing, 101300, PR China

<sup>b</sup>Faculty of Engineering, University of Nottingham, Nottingham, United Kingdom

---

## ARTICLE INFO

*Keywords:*

Carbon fibre

Polymer-matrix composites (PMCs)

Mechanical properties

3D printing

Additive manufacturing

---

## ABSTRACT

Continuous Fibre composite 3D printing (CF-3DP) technology is a newly developed Additive Manufacturing (AM) process. By employing continuous fibre as a reinforcement for the composite, the mechanical properties of the 3D printed part can be significantly improved. However, owing to the process's early stage of development, the mechanical performance of the printed material is still unable to compete with composites produced using conventional manufacturing processes. This can mainly be attributed to lower fibre volume fractions and/or higher void content. The grand objective of the research project is to establish a demonstrator of practical applications, and in this paper, preparatory developments were carried out to pave the ground for the subsequent developments, including feedstock materials development, printing process development, and materials properties evaluation. Efforts have been made to increase fibre volume fraction, to reduce voids content, to evaluate effective properties systematically. The static mechanical test results showed relatively good longitudinal tensile properties while matrix sensitive properties were low, as to be expected in UD composites with a relatively weak matrix material. The advantage of CF-3DP is to achieve fibre steering, and the steered fibre design can be achieved by the current process to realize novel composite structures in future study.

---

## 1. Introduction

Fused Filament Fabrication (FFF), also known as fused deposition modelling (FDM), is an extrusion based 3D printing method [57] that is being considered for end use fabrication, i.e. additive manufacturing (AM). A thermoplastic filament is fed into a heated nozzle where the plastic is melted. The melted plastic is then extruded from the nozzle forming extruded lines and layers while the printhead is moving. 3D objects can be built layer by layer. This process has the advantages of being able to create geometrically complex, customized polymeric parts without the cost of tooling, thus minimising the product development cycle period and material wastage [20]. However, the 3D

---

\* This document is the results of the research project funded by the program of China Scholarships Council (CSC) No.201505870030.

\*Corresponding author

\*\*Principal corresponding author

✉ zhuop@avic.com (P. Zhuo); Shuguang.Li@nottingham.ac.uk (S. Li); Ian.Ashcroft@nottingham.ac.uk (I.A. Ashcroft); ezaij1@exmail.nottingham.ac.uk (A.I. Jones)

ORCID(s): 0000-0001-7511-2910 (P. Zhuo)

printed parts typically have low mechanical properties and have hitherto been largely limited to prototyping rather than the production of functional components. To improve the viability of FFF for the manufacture of structural parts, a number of attempts have been made to improve the mechanical performance of the 3D printed parts by adding discontinuous fibres and particulate reinforcements to the plastic feedstocks [46, 45, 58, 34, 36, 51, 32, 33, 22]. Although 3D printed short fibre reinforced polymer composites show significant improvements in performance over pure plastics, the mechanical properties are still far inferior to those achievable with composites containing continuous fibre reinforcement.

Christian et al. (1998) developed a process combining a form of FFF with continuous fibre reinforced thermoplastic tow placement [11], which was possibly the first CF-3DP technology. Since then, a number of further studies have been carried out in this area and the technology has developed progressively. Unlike feedstock for the FFF printing of pure plastics, fibre reinforcement cannot be used directly for printing as it is not fusible and on its own lacks any structural integrity. It therefore needs to be impregnated with the matrix material for it to be of use in continuous fibre printing. Consequently, various processes and apparatus have been developed aimed at impregnating the fibres before printing. A direct way of impregnating continuous fibres for use in FFF is through an extrusion process to impregnate dry fibres with thermoplastic polymer. An in-nozzle impregnation technique where continuous dry fibres and the thermoplastic matrix filament were fed into the print head simultaneously in designated proportions [44, 39]. The thermoplastic polymer was heated above its melting point in the nozzle, while the dry fibres were pre-heated before entering the nozzle and then impregnated by the molten thermoplastic within the nozzle. The impregnated fibre tow was pulled out of the nozzle while the plastic matrix was extruded from the nozzle and deposited directly to facilitate a 3DP process. A similar process was used in other studies where various matrix materials and types of printhead were used [60, 68, 59, 7, 56, 3, 54]. Li et al. used microwave instead of electronic heating to melt the thermoplastic matrix material in the in-nozzle impregnation printing process [29]. However, a common drawback of the in-nozzle impregnation process was that only a very low fibre volume fraction (lower than 10% [44, 60, 68, 7]) could be achieved. Defects, such as voids and dry fibres, were commonly found, which were probably caused by the difficulty in impregnating the dry fibre tow due to the high viscosity of the molten thermoplastics, the extremely short impregnation times and a lack of compaction during the printing process. Since it is difficult to impregnate the fibres in an in-situ printing process, attempts have been made using pre-impregnated filament (prepreg) materials [11, 63, 26, 38, 50, 31, 64]. In these works, a continuous fibre tow was passed through a molten thermoplastic path to form a tow-preg, and then the prepreg filament was fed into the FFF printer for the printing process. The Markforged Company developed a commercial CF-3DP printer using fibre reinforced nylon prepreg materials as the feedstock materials [37]. As well as in-house manufactured feedstock prepreg materials, researchers have utilized conventional thermoplastic prepreg sheets and cut them into small width tapes for 3DP [48, 67]. Besides in-nozzle impregnation and the use of prepregs,

commingled fibres, which are commonly used in textile composites, have also been utilized for continuous fibre printing [66, 17, 18, 55]. In these studies, commingled fibre tows of reinforcing fibres and thermoplastic fibres are pultruded from a heated metal die and consolidated into a rod-shaped filament to be used as the feedstock materials in the FFF printing process. In some other studies [6, 23, 42, 43, 52], dry fibres were firstly impregnated with low viscosity thermosetting resin. Then the prepreg materials were fed into a printer for the printing process. The impregnated fibre was heated up, softened and laid down on the print bed. After the part was printed, it was moved to a high temperature chamber for curing.

The mechanical performance of the CF-3DP composites have been investigated in a number of studies, including tensile [8, 65, 28, 27, 21, 1, 41, 13, 49, 24], compressive [27, 14], shearing [27, 10], flexural [8, 21, 4, 24], impact [9], interlaminar fracture toughness [24] and fatigue properties [2]. Most of these studies made use of the Markforged printer and the Markforged prepreg materials. By changing the number of fibre layers, fibre types and the infill patterns, different mechanical properties were obtained. Other studies using self-developed printers and materials have mostly performed unidirectional tensile [68, 12, 44, 60, 47, 25, 67, 50, 31, 6, 5, 23, 18, 11, 15, 48, 16, 7] and bending [68, 30, 35, 26, 60, 23, 31, 25, 50, 43, 48] tests to evaluate mechanical performance of the CF-3DP composites. A more complete review is presented in a previous review study [submitted to Composites Part B, under review] and here is only a summary. Overall, the tensile strength and modulus of 3D printed carbon fibre composites vary from a wide range of value widely (e.g. from 147MPa [68] to 1400MPa [67] for tensile strength and from 4GPa [68] to 160GPa [23] for tensile modulus). Since different reinforcement and matrix materials, different printing processes and different fibre volume fractions were used in the various studies above, the mechanical properties achieved in these studies also showed large diversity. In most of these studies, fibre volume content was below 50%, with the exceptions being those which used conventional prepreps or commingled fibres as the feedstock materials [67, 31, 18]. In addition, insufficient impregnation of fibres, high void content and uneven fibre distribution were observed in many CF-3D printed specimens [11, 60, 6, 66, 26, 67, 64, 56, 18, 39]. Lack of compaction during the printing process can be one of the reasons for such defects occurring in the printed parts, resulting in low tensile properties. Utilizing a compaction roller during the printing process [47] or having a post-processing process such as a hot-press showed improvement in the mechanical properties [67]. As a result of these inherent defects, the mechanical properties of the current CF-3DP composites are usually too poor to be considered as a suitable replacement for traditionally processed continuous fibre composites, despite improvements compared to printed pure plastics or short fibre reinforced plastics.

In this study, a carbon/PA6 commingled fibre tow was processed in order to provide the CF-3DP feedstock material. An automated pultrusion process was developed to manufacture the pre-impregnated filament for the printing process. An open-source FFF printer designed for pure plastic printing was adapted for the CF-3DP process. Mechanical test coupon specimens were produced using the pultruded commingled fibres and the modified open-source printer. The

fibres' impregnation quality in the printed specimens was examined. Longitudinal and transverse tensile, longitudinal compressive, bending and shear tests were performed to characterise the basic mechanical performance of the CF-3DP composite materials. A new design philosophy for composite structures has been proposed, in order to exploit the emergence of the CF-3DP technology. The mechanical test results will be used for the Finite Element Analysis (FEA) of new designs in the next part of this study.

## 2. Materials

As discussed in the introduction, the in-nozzle impregnation process suffers from poor impregnation quality and low fibre volume content, while it proved difficult to split conventional prepreg tapes into small widths (smaller than 1mm) in order to produce filament with practical length without breakage. To produce suitable continuous fibre feedstock materials for the printing process with good impregnation quality, 3K carbon/PA6 commingled fibre tow from Concordia USA [19] was used in this study.

The original commingled fibres could not be directly used in the printer for the printing process due to lack of impregnation and practicality, given the primitive printer. Therefore, a pultrusion process has been applied to them to form an appropriate prepreg prior to the subsequent printing. However, this does not exclude the possibility of integrating these two steps in future with an appropriately developed printer for this purpose. A pre-treating pultrusion process was developed for the commingled fibre tow to produce the pre-impregnated continuous fibre feedstock material as shown in Fig.1(a). The commingled fibre tow first passed through a PTFE thermal isolator tube and then a pre-heating tube made of brass, which was at about 200°C. Then the commingled fibre tow passed through a pultrusion die with tapered bore at 250°C within which the thermoplastic fibres were melted so that they would impregnate the carbon fibres. Once the fibre tow passed through the heating zone, it started cooling down and solidified. Then an automated collecting mechanism was employed to collect the consolidated commingled fibre filament. The pultrusion process was repeated three times with three dies of different outlet diameters to achieve full fibre impregnation. The pultruded commingled fibre filament is shown in Fig.1(b).

## 3. The printer and printing process

An open-source RepRap [53] based Velleman K8400 3D printer with two nozzles was adapted for continuous fibre filament printing. One of the nozzles was replaced by a specially designed one for printing the pultruded commingled fibre filament. The open-source printer allows the user to control the printer using G-code [53], so the fibre printing path can be arranged freely. A fibre layer pattern was firstly drawn using the CAD software. Then the coordinates of each point in the fibre pattern were extracted and stored in the desired order of printing. After that, the coordinates were used to generate the print file by adding additional G-code commands for the printing process.

In the continuous fibre printing process, a 0.2mm thick polyamide (PA6) substrate of the shape of the first fibre layer needed to be printed first, because the continuous fibre filament could not be printed directly onto the print bed as the fibre filament could not adhere to it. This substrate consisted of 2 layers of pure plastic and was produced by conventional FFF printing. After the plastic substrate was printed, the continuous fibre filament was manually fed into the fibre nozzle and the fibre layer printing file was selected in the printer's menu to start the printing. Once the fibre nozzle reached the desired temperature, the printhead moves to the starting point above the substrate and the print bed is raised to the height where the distance between the substrate and the nozzle is equal to the layer thickness. On printing, the melted thermoplastic matrix in the fibre filament bonded with the plastic substrate. Once the printhead started moving, the printed fibre filament away from the heating nozzle started cooling down, and the melted thermoplastic matrix solidified and remained bonded to the substrate. Thus, the fibre filament was continuously being pulled out of the printhead from the nozzle as the printhead moved. Once one continuous fibre path finished printing or a layer was finished, the print bed was programmed to move downwards. The fibre filament was cut manually at the end of the path with a pair of scissors. Then the print head moved to a new starting point and a new print layer started according to the pre-designed printing G-code file.

#### 4. Test methods and specimen manufacture

A Zeiss axiolab optical microscope A1 was used to examine the impregnation quality and estimate the fibre volume content and void content of both the pultruded commingled fibre filament and the CF-3DP samples. The sectioned fibre filaments and printed samples were first cast in epoxy resin. The surfaces of the samples were then polished using several different grades of abrasive silicon carbide papers. Optical microscopic images of the samples' cross-sections were then taken.

Tensile, compressive, bending and shear tests were undertaken to characterise the mechanical performance of the continuous fibre 3D printed composites produced using the CF-3DP technology developed. The dimensions of the specimens and the corresponding test standards are listed in Table 2. Specimens were produced using the modified open-source printer and the pultruded commingled fibre filament as the feedstock material. Three specimens were printed for each test using the printing process parameters listed in Table 3. A post-processing stage was carried out to improve impregnation of carbon fibres and bonding between layers, reduce void content and increase crystallinity to achieve better mechanical performance. The printed specimens were vacuum bagged on a metal plate, as shown in Fig.2(a), and vacuum was applied on the specimens. The plate with the specimens was then placed in a pre-heated oven for 15 minutes at 220°C. After post-processing, aluminium end tabs were bonded to the tensile and compressive test specimens to aid gripping. The final specimens are shown in Fig.2(b). An Instron servohydraulic testing machine (Instron Ltd) was used to perform the mechanical testing, and an AVT Stingray F-146B camera (Allited Version Tech-

nologies) and the imetrum video gauge (Imetrum Ltd) was used for strain measurement. One side of each specimen was spray-painted with random black and white speckles to act as a reference surface for the strain measurement.

## 5. Results and discussion

### 5.1. Fibre volume fraction

Firstly, the original condition of the commingled fibres tow was examined using an optical microscope, as shown in Fig.3. The diameters of the fibre cross-sections were measured using software ImageJ. The circles with bigger diameter (40 $\mu$ m) were the PA6 fibres, while the small dots (diameter 7 $\mu$ m) were the carbon fibres. As can be seen from the picture, the carbon fibres and PA6 fibres were not well distributed and there was little presence of PA6 fibres within the carbon fibre cluster. Also, the original commingled fibre tow had a wide tape-shaped cross section, approximately 2mm wide and 0.6mm thick. The number of PA6 fibres was counted to be 73 in the optical microscope picture. In the fibre volume calculation, an approximate carbon fibre number of 3000 was used as the commingled fibre material was a 3K carbon fibre tow. The total volumes of carbon fibres and PA6 fibres in one single tow were calculated from their fibre counts and diameters and are listed in Table 1. The volume of a fully impregnated fibre filament would be the sum of the volume of carbon fibres and PA6 fibres. Therefore, the fibre volume fraction of the original commingled fibre was calculated to be 55% using Equation 1.

$$V_f = \frac{n_{carbon} \cdot \pi \left(\frac{D_{carbon}}{2}\right)^2}{n_{carbon} \cdot \pi \left(\frac{D_{carbon}}{2}\right)^2 + n_{PA6} \cdot \pi \left(\frac{D_{PA6}}{2}\right)^2} \times 100\% \quad (1)$$

Then, the commingled carbon/PA6 feedstock material was examined directly after pultrusion in order to evaluate its suitability as a feedstock material for FFF. Filaments were sectioned and examined under an optical microscope. As can be seen in Fig. 4(a) and (b), the carbon fibre distribution was not uniform across the filament cross section. Fibres congregated near the edge of the filament surface, leaving a resin rich area in the centre of the filament, which was believed to be caused by the pultrusion process. During the process, the carbon fibres were pulled through a tapered bore where the PA6 plastic melted to enable flow. Thus, due to the decrease of cavity size as the commingled fibres passed through the tapered bore, the carbon fibres tended to move closer to the inner wall of the tapered bore while the melted PA6 was squeezed into the centre, as can be seen in Fig.4(a). Cavities were observed inside some of the filament cross-sections, as shown in Fig.4(b) and (d). Some voids were also observed among the carbon fibre bundles, as shown in Fig. 4(c) and (d). These defects might be due to a combination of causes, including insufficient pressure, poor fluidity of the thermoplastic and moisture vaporizing in the PA6 polymer. The cross-section image of the pultruded commingled fibre filament was used to estimate the fibre the fibre volume fraction and void content using

the ImageJ software, giving values of 47.74% and 5.36% respectively.

The printed specimens were examined using an optical microscope after the thermal post treatment described in Section 4. The optical microscopic images of the sample cross-section are shown in Fig.5. Images were taken of the same region under 25 times, 50 times and 100 times magnifications. The white circles are the carbon fibres, the PA6 matrix is the grey colour and the voids are in black. As can be seen in Fig.5(a), the individual fibre tows can be identified. Also, a resin rich area in the space between four adjacent filaments was observed. Some voids were found within the fibre filaments and between layers. From the observation of the optical microscope images, the print quality of the printed sample was judged to be satisfactory. No gaps or insufficient bonding between filaments and layers were observed. Very few dry fibres were found within the filaments. The fibre volume fraction and void content of the printed sample were measured using the Image-J software. The measurement results are listed in Table 4. The convention used in Fig.5(d), (e), (f) is that the matrix area is marked red and the voids are marked black. The fibre volume content and the void content of the region were measured to be around 45% and 0.6% respectively. It was noted that although the fibre volume content was slightly lower than the pultruded commingled fibre filament, the void content was much lower. Since the printed samples had extra layers of pure PA6 on both surfaces which were re-melted during the post-processing process, fibres were able to penetrate into these pure plastic layers, which is the probable cause of lower fibre volume content in the printed sample. Furthermore, the post-processing stage had a positive effect in reducing the void content in the printed samples. The printed specimens showed good microstructure after post-processing. However, the fibre volume fraction currently achieved did not reach the target value (50% or higher) desired for printed composites. In order to achieve this target, the fibre volume fraction of the feedstock material needs to be increased.

## 5.2. Tensile testing

### 5.2.1. 0° tensile test

The 0° (longitudinal) tensile test specimens consisted of 2 fibre layers and 2 PA6 top and bottom layers. Two groups of specimens were prepared, one without post-processing and the other with post-processing. The testing setup and a failed specimen are shown in Fig.6(a) and (b). The 0° tensile test results are listed in Table 5, and the stress-strain curves of the two groups are shown in Fig.7(a) and (b). The mean maximum 0° tensile strengths of the 3D printed continuous fibre composite specimens with and without post-processing were 859MPa and 712MPa respectively. The mean 0° tensile modulus of the 3D printed continuous fibre composites with and without post-processing were 61.1GPa and 57.4GPa respectively. The specimens with post-processing showed 20.6% and 6.43% improvement in tensile strength and modulus respectively, compared to specimens without post-processing, while the thickness of the specimens with post-processing was 5% smaller than that of the specimens without post-processing. In addition, in comparison to

the literature, the tensile strength and modulus of the specimens with post-processing were 22.8% and 22.1% higher compared to those produced using the commercial printer [37].

The fractured specimens after the tensile test are shown in Fig.8. The specimens without post-processing showed fibre splitting and de-bonding between the surface plastic layers and the fibre layers, as can be seen in Fig.8(a). Delamination can be observed from the side of the samples. Additionally, dry fibres were found at the failure sections of the specimens without post-processing. The specimens with post-processing exhibited long splitting failure and angled breakage but not delamination, as shown in Fig.8(b). Some dry fibres were found at the failure sites but much less than in the specimens without post-processing. The examination of fracture surfaces indicates that the post-processing process resulted in better fibre impregnation and layer bonding.

### 5.2.2. 90° Tensile test

A laminate of 180mm×120mm×2mm was printed, which consisted of 6 fibre layers and 2 PA6 layers on both top and bottom. The fibre was printed along the transverse direction. The laminate was post-processed before cutting into the final dimensions of the specimens. 3 specimens were cut from the laminate using a water jet cutter. All specimens tested in the 90° tensile test were post-processed since specimens without post-processing suffered from very weak bonding between printed filaments.

The same testing setup was used as for the 0° tensile test. The results of the 90° tensile tests are listed in Table 5 and the stress-strain curves are shown in Fig.9(b). The mean 90° tensile strength of the continuous fibre 3D printed composites is 8.66MPa and the mean modulus is 0.381GPa. The modulus values were calculated using the initial slope, which was from 0.1-0.5% strain. The failure strain of the 90° tensile test specimens was very high, and exhibited large deviation. The high failure strain could be due to the matrix PA6 material which is a tough polymer of high elongation at yield. The large deviation of failure strain could be caused by uneven fibre distribution and insufficient bonding between fibres and matrix material. The failure strength of the 90° tensile test did not reach the failure strength of the matrix PA6 material, which indicated that the failure took place at the interface between the fibres and matrix. Poor bonding would lead to a relatively low failure strain. The tensile strength and modulus values are much lower than reported properties of the pure PA6 matrix, with tensile strength of 45.5MPa, and tensile modulus of 1GPa [40]). The fracture surfaces of the tested specimens are shown in Fig.10. Two specimens failed close to the tabs and one failed in the middle section. All three specimens showed an angled fracture surface through the thickness. Dry fibres were found on the fracture surfaces indicating poor bonding.

Both the low 90° tensile properties and the dry fibres at the fracture surface indicate insufficient bonding between fibres and matrix and between printed fibre tows. These results would not be acceptable if the material were to be used for structural applications. Appropriate values for a structural composite would be in the region of 50MPa for

90° tensile strength and 5GPa for 90° tensile modulus, which are approximately an order of magnitude greater than the measured values here. Further investigation is required to examine if the sizing on the carbon fibre is compatible with the PA6 matrix, if post-processing time was sufficient, and more repeats of the test are needed to see if the value obtained is valid and repeatable. Better impregnation in the prepreg feedstock and appropriate compaction during printing are therefore essential aspects for future improvement if the technology is to evolve to its maturity.

### 5.3. Compressive testing

Three specimens with post-processing were prepared for the in-plane compressive test. The loading direction was along the fibre direction of the specimens. Each specimen consisted of 6 fibre layers and 2 PA6 layers on top and bottom surfaces. One side of each specimen was spray-painted with random black and white speckles for strain measurement. The specimens were mounted in the compressive test fixture as shown in Fig.11(a), and the fixture was placed in the Instron testing machine. The gauge length between the end tabs was 10mm, and the testing rate was set to 1mm/min.

The stress-strain curves for the compressive test are shown in Fig.11(b), and the test results are listed in Table 5. The mean values of the maximum in-plane compressive strength and modulus of the continuous fibre 3D printed composites were 379MPa and 65.8GPa respectively, which were 23.16% and 31.52% higher than those of material produced using the commercial printer [37]. In addition, the compressive properties are comparable with those of composites made from carbon/PA6 UD tapes (compressive strength 375MPa with fibre volume fraction of 48% [40]). The measured compressive modulus was close to that obtained under tension while the strength differs as expected due to fibre instability in the compressive test. All specimens showed through-thickness angled failure close to the tabs.

### 5.4. Bend testing

The 4-point bending specimens consisted of 5 fibre layers and 2 PA6 top and bottom layers. Fibres were along the longitudinal direction. The testing setup is shown in Fig.12(a). A deflection gauge was placed under the specimen to measure the flexural strain up to 0.5%, which was used for modulus calculation. After that, the gauge was removed from the setup and the test continued until the specimen failed as shown in Fig.12(b). The maximum flexural stress  $\sigma$  was calculated using Equation 2, where  $P$  is the applied force,  $L$  is the support span,  $b$  is the width of beam, and  $h$  is the thickness of beam. The 4-point bending test results are listed in Table 5, and the stress-strain curves of the 4-point bending test are shown in Fig.13(a).

$$\sigma = \frac{3PL}{4bh^2} \quad (2)$$

The mean maximum flexural strength and the mean flexural modulus of the printed specimens were 600MPa and

54.4GPa respectively. The flexural properties of the specimens manufactured in this work were 71.8% and 80.2% higher in terms of strength and modulus respectively over those reported with the commercial printer [37]. However, flexural strength of conventionally manufactured composites with 48% fibre volume fraction made directly from carbon/PA6 UD tape has been reported as 950MPa [40], which is 37% higher than that achieved in this study. Fibre breakage was found on the fracture surfaces, as shown in Fig.13(b). Dry fibres and pulled-out fibres were observed on the tensile side of the specimens. These un-impregnated fibres could be the cause of the low mechanical properties. Better sizing to improve wetting of the fibre is required, and the pultrusion process needs to be improved to achieve better fibre impregnation.

### 5.5. Shear testing

A  $180\text{mm} \times 140\text{mm}$  laminate was printed to produce four V-Notched Rail Shear testing specimens. The laminate consisted of 8 fibre layers with the layup sequence of  $[0/90]_{2s}$  sandwiched between top and bottom layers of pure PA6 layers. The laminate was post-processed before machining. Three specimens were cut from the laminate using a water jet cutting machine.

During the test, the sides of the specimens were clamped by two L-shaped fixtures as shown in Fig. 14(a). The displacement rate was set to be  $1\text{mm}/\text{min}$ . The shear strain was obtained by adding the absolute values of the strains in the  $\pm 45^\circ$  directions,  $\epsilon_{+45}$  and  $\epsilon_{-45}$ , using Equation 3. Four target points were chosen as shown in Fig. 14(b).  $\epsilon_{+45}$  was the strain between target 1 and 2, and  $\epsilon_{-45}$  was the strain between target 3 and 4. Shear stress was calculated as the loading force divided by the cross sectional area between the notches. The ultimate shear strength  $\tau_u$  is obtained by Equation 4, where  $F_u$  is the force at 5% engineering shear strain, given that the stress-strain curve is found to be asymptotic rather than exhibiting a peak.

$$\gamma = |\epsilon_{+45}| + |\epsilon_{-45}| \quad (3)$$

$$\tau_u = \frac{F_u}{A} \quad (4)$$

Three specimens were tested and one was kept as a spare in case an undesired test failure occurred. The test results are listed in Table 5, and the stress and strain curves of the V-notched rail shear test are shown in Fig. 15. Fibre rotation was observed during the test. This rotation allowed the fibres to carry the force after shear failure, leading to curves which are asymptotic with no clearly-defined maximum stress. The mean ultimate shear strength was 23.4MPa, and the mean shear modulus was 1.05GPa. These values are lower than expected; for example, for carbon/epoxy prepreg composites with 60% fibre volume fraction, the expected in-plane shear strength is  $98\text{MPa}$  [62], which is three times higher than the test results in this study.

The test failed specimens from the V-notched rail shear test are shown in Fig.14(c). Horizontal cracking at gauge section between notches failure mode was found in all three specimens. Fibre breakage was observed and the  $0^\circ$  fibres were seen to have rotated by about  $20^\circ$ . Wrinkles were found on the surfaces of the failed specimens as shown in Fig. 14(d). Dry fibres were observed on the fractured surfaces, indicating poor wetting of the fibres by the molten matrix during manufacture, which would account for the low in-plane shear properties.

## 5.6. Mechanical test results summary and discussion

As mentioned in the introduction section, most studies in the literature mainly investigated tensile and flexural properties of the CF-3DP composites. Thus, the tensile and flexural performance of the CF-3DP composites obtained in this study is compared with those from the literature. The figures that summarized the tensile and flexural properties of the CF-3DP composites in the literature are shown in Fig.16(a) and (b) respectively. Each label represents a data point of the properties obtained from a literature. The full figures with legends showing the reference of each data point can be found in the previous review study[70] recently published in Composites Part B. The data obtained in this study is pointed out and labelled as red stars. The tensile and flexural properties obtained in this study are superior to those manufactured by the commercial printer and those in most of the literature for CF-3DP. However, they still have not achieved the level of properties expected for carbon fibre composites materials manufactured by conventional methods.

The fibre volume fraction of the printed specimens achieved in the current study was around 45% and the average value of the  $0^\circ$  tensile modulus was 61.1GPa. If rule of mixture was applied to estimate the sample with 50% fibre volume fraction, its modulus would be 67.9GPa, which is relatively low compared to composite materials produced using conventional methods. It should be pointed out that the tensile test specimens produced using the continuous fibre 3D printing technology in this study consisted of 0.4mm thick PA6 plastic surfaces (0.2mm on each side) which is 40% of the total thickness, and the carbon fibre layers thickness was 0.6mm. If the plastic surface layers are ignored and only the thickness of the fibre layers is used to calculate the tensile strength of the CF-3DP composite specimens, it would result in a strength of 1432MPa. Compared to the tensile strength of the carbon/PA6 UD tapes composites with 48% fibre volume fraction (1900MPa) [61], the tensile strength of the CF-3DP composite specimens in the current study is still 24% lower. The fibre volume fraction of the specimens in the current study is only marginally lower and this discrepancy would not account for the 24% difference. Other reasons causing the low tensile strength results could be fibres not perfectly aligned at  $0^\circ$ , along with fibre waviness or fibre twisting in the printed specimens. In order for the CF-3DP composites to be applied in structural applications, the fibre volume fraction needs to be increased to 55% or higher (especially for aerospace application), and mechanical properties need to be improved, for example to 2000MPa and 120GPa respectively for  $0^\circ$  tensile strength and modulus). In addition, fibre wetting and impregnation

need to be improved as dry fibres were commonly found in the failed specimens.

The current approach using vacuum bagging to compress the printed specimens is one way to improve bonding between layers. It was also beneficial to increase crystallinity and hence increase mechanical performance. However, this method might not be necessarily practical in all 3D printed situations as it is likely to distort the printed component geometry. Another way to improve bonding would be using a compaction roller or similar, which would be able to apply compaction force during the printing process. This in-situ compaction process would be dynamic and possible to follow the contour of the printed part. However, the process parameters such as force, speed, temperature and etc. might need to be investigate. In order to achieve the desirable fibre volume fraction, better layer bonding and homogeneous fibre distribution for structural composites, both in-situ compaction during printing and high compaction pressure post-processing might be required, though part distortion under the compaction forces would need to be avoided.

## 6. Design of a structural part as an application of CF-3DP

Although the mechanical performance of CF-3DP composites at the current stage cannot compete with that of composites produced using conventional manufacturing methods, it does not diminish the process's key advantage of being able to achieve manufacture parts with fibre paths optimised for specific loading conditions. The open-source printer allows the user to control the printer using G-code so that the fibres in one layer do not have to be in a uniform direction, thus introducing much more design freedom for composite materials. One specific application for CF-3DP will be key load bearing composite parts with features such as holes or notches. In conventional composite materials, where fibres are laid along straight paths, holes or notches usually need to be machined afterwards, inevitably disrupting fibre continuity and causing significant edge effects, which encourages premature failure while weakening the part under consideration. Maintaining the continuity of the fibres is extremely beneficial to avoid strength loss due to fibre discontinuity. Steering fibres around holes or notches to avoid the fibres being cut is a potential solution to achieve better performance for such composite parts. While the capability of designing steered fibre paths remains the ultimate goal of the authors, an appropriate composite manufacturing technology is required to realize the design philosophy, which is the authors' intended purpose for which the CF-3DP technology has been developed. The technology developed so far, though far from being mature, has allowed the authors to further explore the design philosophy by guiding the fibre path according to the prime loading conditions.

At the current stage, the CF-3DP technology was developed by establishing a suitable feedstock material for the printing process and adapting an open-source FDM printer to achieve the required capability of fibre steering. Coupon specimens were manufactured and tested in this study, which provided a basic knowledge of the mechanical performance of the CF-3DP materials at the current level of development. Previously, a preliminary fibre path design was proposed for a single hole lug by the authors [69], as shown in Fig.17(a) and (b). Unlike in conventional quasi-isotropic

composites laminate, where fibres would be truncated at the hole boundary, fibres were designed to pass around the hole to maintain fibre integrity, as shown in Fig.17(a). At the same time, arch-shaped columns were introduced under the hole to sustain the compressive load, as shown in Fig.17(b) with necessary fibre tows for sideways binding effects (not shown), e.g. in  $\pm 45$  directions. The use of arches is to moderate the stiffness of the contact area at the hole edge, spreading the compressive load so that, in the aim of optimizing the design, the structure will be sustained by a desirably less stiff contact. Usually, key load bearing structural parts are strength controlled and there is excess stiffness, which can potentially be sacrificed to reduce the concentration of the bearing load. Following the proposed design philosophy, curvilinear fibre patterns were designed for the lug shape samples as shown in Fig.18. In group 1, fibres were designed going around the hole to sustain the pulling force, while several small support columns were designed under the hole to sustain the pushing load. In group 2, the fibre patterns are designed for compressive loading condition mainly. A full ring with the diameter of the net section is designed at the top part of the pattern, and multiple columns are designed below the ring. Fibre patterns in group 3 are the combination of Pattern group 1 and Pattern group 2. A ring with the diameter of half of the net section is designed around the hole, and several columns are designed below the ring, which is the same as the pattern group 2. In the meantime, fibres are designed going around the hole similar to Pattern group 1. Finally the Patterns 4-1 and 4-2 are mainly composed of  $\pm 45$  and  $\pm 45$  but without fibres cut at the hole.

Lug samples with curvilinear fibre path and with quasi-isotropic layup design were produced using the CF-3DP technology, as shown in Fig.19(a) and (b). The details of the design, manufacturing process and testing will be presented in the study where one lug sample was tested in tension and the other was tested in compression and compared with samples with a quasi-isotropic layup. FEA will also be used to support the lug design with consideration of curvilinear fibre paths, using the mechanical properties obtained in the current coupon tests.

## 7. Conclusions

A CF-3DP process was developed in this study. A pultrusion process was developed to manufacture the feedstock material for the printing process using a 3k carbon/PA6 commingled fibre tow. A RepRap based open-source FFF printer was modified to enable continuous fibre printing. Coupon specimens were produced using the pultruded commingled fibres and the modified FFF printer, and they were post-processed in an oven with vacuum applied to improve the quality. The printed specimens were examined using an optical microscope. The fibre volume content was estimated to be 44-47% and the void content was 0.5-2.0%. Tensile, compressive, bending and shear tests were performed to investigate the mechanical performance of the CF-3DP composite materials. The results showed relatively high strength in the fibre direction, but very low values for the matrix sensitive properties such as tensile strength in the transverse direction. Un-impregnated fibres were found in the fracture surfaces of the failure specimens. Nevertheless,

the longitudinal tensile properties obtained in this study are higher than those of material manufactured by the commercial printer and those in most of the literature, owing to a higher fibre volume and lower void content. However, this performance is still not comparable with composites manufactured by conventional methods. Improvements in feedstock materials, fibre volume fraction, fibre impregnation and printing process need to be achieved before the large gap between the CF-3DP composites and conventional composites can be filled sufficiently that the CF-3DP composites can be applied in high performance structural components.

The grand objective of the research project the authors have been pursuing is to establish a demonstrator of practical applications. In order to do so, some preparatory developments were necessary to pave the ground for the subsequent developments. Such preparatory developments must be recorded in a creditable manner which is the purpose of this manuscript so that the next paper would be allowed to concentrate on subject of practical applications through a demonstrator. The manufacturing process developed in this study has its similarity with the existing ones. However, the achievements as presented in the manuscript are not a trivial exercise. Efforts has been made to increase fibre volume fraction, to reduce voids contents, to evaluate effective properties systematically, etc. These are all essential measures to promote practical applications. Whilst these are not meant to be revolutionary, each of them represents an incremental progress made in this direction and hence the novelty. The authors believe that, for a creditable establishment of the grand objective, it is helpful to publish the preparatory developments and the subsequent structural design exercise separately so that they will support each other, rather than obstructing each other in demonstrating the achievement of the grand objective.

## 8. Acknowledgements

This research is supported by the program of China Scholarships Council (CSC) No.201505870030. The authors would like to express the appreciation to Azamat Keulimzhaiuly, Adhith T Rajeshand, Siyu Liu for their valuable contributions, and all the research technicians Paul Johns, Ben Jennison, Jason Greaves and Graham Malkinson for their technical support in this research work.

## References

- [1] Abadi, H.A., Thai, H.T., Paton-Cole, V., Patel, V., 2018. Elastic properties of 3d printed fibre-reinforced structures. *Composite Structures* 193, 8–18. doi:10.1016/j.compstruct.2018.03.051.
- [2] Agarwal, K., Kuchipudi, S.K., Girard, B., Houser, M., 2018. Mechanical properties of fiber reinforced polymer composites: a comparative study of conventional and additive manufacturing methods. *Journal of Composite Materials* 52, 3173–3181. URL: <https://doi.org/10.1177/0021998318762297>, doi:10.1177/0021998318762297, arXiv:<https://doi.org/10.1177/0021998318762297>.

- [3] Akhoundi, B., Behraves, A.H., Saed, A.B., 2018. Improving mechanical properties of continuous fiber-reinforced thermoplastic composites produced by FDM 3d printer. *Journal of Reinforced Plastics and Composites* 38, 99–116. doi:10.1177/0731684418807300.
- [4] Araya-Calvo, M., López-Gómez, I., Chamberlain-Simon, N., León-Salazar, J.L., Guillén-Girón, T., Corrales-Cordero, J.S., Sánchez-Brenes, O., 2018. Evaluation of compressive and flexural properties of continuous fiber fabrication additive manufacturing technology. *Additive Manufacturing* 22, 157–164. doi:10.1016/j.addma.2018.05.007.
- [5] Azarov, A.V., Antonov, F.K., Golubev, M.V., Khaziev, A.R., Ushanov, S.A., 2019. Composite 3d printing for the small size unmanned aerial vehicle structure. *Composites Part B: Engineering* 169, 157–163. doi:10.1016/j.compositesb.2019.03.073.
- [6] Azarov, A.V., Antonov, F.K., Vasil'ev, V.V., Golubev, M.V., Krasovskii, D.S., Razin, A.F., Salov, V.A., Stupnikov, V.V., Khaziev, A.R., 2017. Development of a two-matrix composite material fabricated by 3d printing. *Polymer Science, Series D* 10, 87–90. doi:10.1134/S1995421217010026.
- [7] Bettini, P., Alitta, G., Sala, G., Di Landro, L., 2017. Fused deposition technique for continuous fiber reinforced thermoplastic. *Journal of Materials Engineering and Performance* 26, 843–848. URL: <https://doi.org/10.1007/s11665-016-2459-8>, doi:10.1007/s11665-016-2459-8.
- [8] Blok, L., Longana, M., Yu, H., Woods, B., 2018. An investigation into 3D printing of fibre reinforced thermoplastic composites. *Additive Manufacturing* 22, 176 – 186. URL: <http://www.sciencedirect.com/science/article/pii/S2214860417305687>, doi:<https://doi.org/10.1016/j.addma.2018.04.039>.
- [9] Caminero, M., Chacón, J., García-Moreno, I., Rodríguez, G., 2018a. Impact damage resistance of 3d printed continuous fibre reinforced thermoplastic composites using fused deposition modelling. *Composites Part B: Engineering* 148, 93–103. doi:10.1016/j.compositesb.2018.04.054.
- [10] Caminero, M., Chacón, J., García-Moreno, I., Reverte, J., 2018b. Interlaminar bonding performance of 3D printed continuous fibre reinforced thermoplastic composites using fused deposition modelling. *Polymer Testing* 68, 415 – 423. URL: <http://www.sciencedirect.com/science/article/pii/S0142941818304264>, doi:<https://doi.org/10.1016/j.polymertesting.2018.04.038>.
- [11] Christian, P., Jones, I., Rudd, C., Campbell, R., Corden, T., 2001. Monomer transfer moulding and rapid prototyping methods for fibre reinforced thermoplastics for medical applications. *Composites Part A: Applied Science and Manufacturing* 32, 969 – 976. URL: <http://www.sciencedirect.com/science/article/pii/S1359835X01000094>, doi:[https://doi.org/10.1016/S1359-835X\(01\)00009-4](https://doi.org/10.1016/S1359-835X(01)00009-4).
- [12] De Backer, W., Bergs, A.P., Van Tooren, M.J., 2018. Multi-axis multi-material fused filament fabrication with continuous fiber reinforcement, in: 2018 AIAA/ASCE/AHS/ASC Structures, Structural Dynamics, and Materials Conference, p. 0091.
- [13] Dickson, A.N., Barry, J.N., McDonnell, K.A., Dowling, D.P., 2017. Fabrication of continuous carbon, glass and kevlar fibre reinforced polymer composites using additive manufacturing. *Additive Manufacturing* 16, 146 – 152. URL: <http://www.sciencedirect.com/science/article/pii/S2214860416301889>, doi:<https://doi.org/10.1016/j.addma.2017.06.004>.
- [14] Dikshit, V., Yap, Y.L., Goh, G.D., Yang, H., Lim, J.C., Qi, X., Yeong, W.Y., Wei, J., 2016. Investigation of out of plane compressive strength of 3d printed sandwich composites. *IOP Conference Series: Materials Science and Engineering* 139, 012017. doi:10.1088/1757-899x/139/1/012017.
- [15] Domm, M., Schlimbach, J., Mitschang, P., 2017. Optimizing mechanical properties of additively manufactured frpc, in: 21st International Conference on Composite Materials, Xi'an, China.
- [16] Duigou, A.L., Barbé, A., Guillou, E., Castro, M., 2019. 3d printing of continuous flax fibre reinforced biocomposites for structural applications. *Materials & Design* 180, 107884. doi:10.1016/j.matdes.2019.107884.
- [17] Eichenhofer, M., Maldonado, J.I., Klunker, F., Ermanni, P., 2015. Analysis of processing conditions for a novel 3d-composite production

- technique, in: 20th International Conference on Composite Materials.
- [18] Eichenhofer, M., Wong, J.C., Ermanni, P., 2017. Continuous lattice fabrication of ultra-lightweight composite structures. *Additive Manufacturing* 18, 48–57. doi:10.1016/j.addma.2017.08.013.
- [19] Fibers, C., . URL: <http://www.concordiafibers.com/index.html>.
- [20] Frketic, J., Dickens, T., Ramakrishnan, S., 2017. Automated manufacturing and processing of fiber-reinforced polymer (frp) composites: An additive review of contemporary and modern techniques for advanced materials manufacturing. *Additive Manufacturing* 14, 69–86.
- [21] Goh, G.D., Yap, Y.L., Agarwala, S., Yeong, W.Y., 2018. Recent progress in additive manufacturing of fiber reinforced polymer composite. *Advanced Materials Technologies* 4, 1800271. doi:10.1002/admt.201800271.
- [22] Griffini, G., Invernizzi, M., Levi, M., Natale, G., Postiglione, G., Turri, S., 2016. 3d-printable cfr polymer composites with dual-cure sequential ipns. *Polymer* 91, 174 – 179. URL: <http://www.sciencedirect.com/science/article/pii/S0032386116301884>, doi:<https://doi.org/10.1016/j.polymer.2016.03.048>.
- [23] Hao, W., Liu, Y., Zhou, H., Chen, H., Fang, D., 2018. Preparation and characterization of 3d printed continuous carbon fiber reinforced thermosetting composites. *Polymer Testing* 65, 29–34. doi:10.1016/j.polymertesting.2017.11.004.
- [24] He, Q., Wang, H., Fu, K., Ye, L., 2020. 3d printed continuous CF/PA6 composites: Effect of microscopic voids on mechanical performance. *Composites Science and Technology* 191, 108077. doi:10.1016/j.compscitech.2020.108077.
- [25] Heidari-Rarani, M., Rafiee-Afarani, M., Zahedi, A., 2019. Mechanical characterization of FDM 3d printing of continuous carbon fiber reinforced PLA composites. *Composites Part B: Engineering* 175, 107147. doi:10.1016/j.compositesb.2019.107147.
- [26] Hu, Q., Duan, Y., Zhang, H., Liu, D., Yan, B., Peng, F., 2017. Manufacturing and 3d printing of continuous carbon fiber prepreg filament. *Journal of Materials Science* 53, 1887–1898. doi:10.1007/s10853-017-1624-2.
- [27] Justo, J., Távora, L., García-Guzmán, L., París, F., 2018. Characterization of 3D printed long fibre reinforced composites. *Composite Structures* 185, 537 – 548. doi:10.1016/j.compstruct.2017.11.052.
- [28] Kvalsvig, A., Yuan, X., Potgieter, J., Cao, P., 2017. Analysing the tensile properties of 3D printed fibre reinforced thermoplastic composite specimens, in: 2017 24th International Conference on Mechatronics and Machine Vision in Practice (M2VIP), pp. 1–6. doi:10.1109/M2VIP.2017.8211514.
- [29] Li, N., Link, G., Jelonnek, J., 2020. 3d microwave printing temperature control of continuous carbon fiber reinforced composites. *Composites Science and Technology* 187, 107939. doi:10.1016/j.compscitech.2019.107939.
- [30] Liu, T., Tian, X., Zhang, M., Abliz, D., Li, D., Ziegmann, G., 2018. Interfacial performance and fracture patterns of 3d printed continuous carbon fiber with sizing reinforced pa6 composites. *Composites Part A: Applied Science and Manufacturing* 114, 368–376.
- [31] Liu, T., Tian, X., Zhang, Y., Cao, Y., Li, D., 2020. High-pressure interfacial impregnation by micro-screw in-situ extrusion for 3d printed continuous carbon fiber reinforced nylon composites. *Composites Part A: Applied Science and Manufacturing* 130, 105770. doi:10.1016/j.compositesa.2020.105770.
- [32] Llewellyn-Jones, T.M., Drinkwater, B.W., Trask, R.S., 2016. 3d printed components with ultrasonically arranged microscale structure. *Smart Materials and Structures* 25, 02LT01.
- [33] Llewellyn-Jones, T., Drinkwater, B., Trask, R., 2017. Mechanical properties of additively manufactured composite materials with ultrasonically assembled reinforcement, in: Proceedings of the 21st International Conference on Composite Materials, ICCM21, ID, Xi'an, China.
- [34] Love, L.J., Kunc, V., Rios, O., Duty, C.E., Elliott, A.M., Post, B.K., Smith, R.J., Blue, C.A., 2014. The importance of carbon fiber to polymer additive manufacturing. *Journal of Materials Research* 29, 1893–1898.
- [35] Luo, M., Tian, X., Shang, J., Zhu, W., Li, D., Qin, Y., 2019. Impregnation and interlayer bonding behaviours of 3d-printed continuous carbon-

- fiber-reinforced poly-ether-ether-ketone composites. *Composites Part A: Applied Science and Manufacturing* 121, 130–138. doi:10.1016/j.compositesa.2019.03.020.
- [36] Mahajan, C., Cormier, D., 2015. 3d printing of carbon fiber composites with preferentially aligned fibers, in: IIE annual conference. Proceedings, Institute of Industrial and Systems Engineers (IISE). p. 2953.
- [37] Markforged, . <https://markforged.com/>.
- [38] Matsuzaki, R., Nakamura, T., Sugiyama, K., Ueda, M., Todoroki, A., Hirano, Y., Yamagata, Y., 2018. Effects of set curvature and fiber bundle size on the printed radius of curvature by a continuous carbon fiber composite 3d printer. *Additive Manufacturing* 24, 93 – 102. URL: <http://www.sciencedirect.com/science/article/pii/S2214860418303294>, doi:<https://doi.org/10.1016/j.addma.2018.09.019>.
- [39] Matsuzaki, R., Ueda, M., Namiki, M., Jeong, T.K., Asahara, H., Horiguchi, K., Nakamura, T., Todoroki, A., Hirano, Y., 2016. Three-dimensional printing of continuous-fiber composites by in-nozzle impregnation. *Scientific reports* 6, 23058.
- [40] MatWeb, . URL: <http://www.matweb.com/index.aspx>.
- [41] Melenka, G.W., Cheung, B.K., Schofield, J.S., Dawson, M.R., Carey, J.P., 2016. Evaluation and prediction of the tensile properties of continuous fiber-reinforced 3D printed structures. *Composite Structures* 153, 866 – 875. URL: <http://www.sciencedirect.com/science/article/pii/S0263822316311497>, doi:<https://doi.org/10.1016/j.compstruct.2016.07.018>.
- [42] Ming, Y., Duan, Y., Zhang, S., Zhu, Y., Wang, B., 2020a. Self-heating 3d printed continuous carbon fiber/epoxy mesh and its application in wind turbine deicing. *Polymer Testing* 82, 106309. doi:10.1016/j.polymertesting.2019.106309.
- [43] Ming, Y., Zhang, S., Han, W., Wang, B., Duan, Y., Xiao, H., 2020b. Investigation on process parameters of 3d printed continuous carbon fiber-reinforced thermosetting epoxy composites. *Additive Manufacturing* 33, 101184. doi:10.1016/j.addma.2020.101184.
- [44] Namiki, M., Ueda, M., Todoroki, A., Hirano, Y., Matsuzaki, R., 2014. 3d printing of continuous fibre reinforced plastic, in: SAMPE, International SAMPE Symposium and Exhibition, Society for the Advancement of Material and Process Engineering (SAMPE), Seattle, WA, US. pp. 1–6.
- [45] Ning, F., Cong, W., Hu, Y., Wang, H., 2017. Additive manufacturing of carbon fiber-reinforced plastic composites using fused deposition modeling: Effects of process parameters on tensile properties. *Journal of Composite Materials* 51, 451–462.
- [46] Ning, F., Cong, W., Qiu, J., Wei, J., Wang, S., 2015. Additive manufacturing of carbon fiber reinforced thermoplastic composites using fused deposition modeling. *Composites Part B: Engineering* 80, 369–378.
- [47] Omuro, R., Ueda, M., Matsuzaki, R., Todoroki, A., Hirano, Y., 2017. Three-dimensional printing of continuous carbon fiber reinforced thermoplastics by in-nozzle impregnation with compaction roller, in: Proceedings of the 21st International Conference on Composite Materials, Xi'an, China.
- [48] Parandoush, P., Tucker, L., Zhou, C., Lin, D., 2017. Laser assisted additive manufacturing of continuous fiber reinforced thermoplastic composites. *Materials & Design* 131, 186–195. doi:10.1016/j.matdes.2017.06.013.
- [49] Peng, Y., Wu, Y., Wang, K., Gao, G., Ahzi, S., 2019. Synergistic reinforcement of polyamide-based composites by combination of short and continuous carbon fibers via fused filament fabrication. *Composite Structures* 207, 232–239.
- [50] Qiao, J., Li, Y., Li, L., 2019. Ultrasound-assisted 3d printing of continuous fiber-reinforced thermoplastic (FRTP) composites. *Additive Manufacturing* 30, 100926. doi:10.1016/j.addma.2019.100926.
- [51] Quan, Z., Larimore, Z., Wu, A., Yu, J., Qin, X., Mirotznik, M., Suhr, J., Byun, J.H., Oh, Y., Chou, T.W., 2016. Microstructural design and additive manufacturing and characterization of 3d orthogonal short carbon fiber/acrylonitrile-butadiene-styrene preform and composite. *Composites Science and Technology* 126, 139–148.

- [52] Ranabhat, B., Kirmse, S., Hsiao, K., 2019. Feasibility study of novel magnetic compaction force assisted additive manufacturing (MCFA-AM) methodology for continuous carbon fiber reinforced polymer (c-CFRP) composites, in: SAMPE 2019 - Charlotte, NC, SAMPE. doi:10.33599/nasampe/s.19.1535.
- [53] RepRap, 2015. Reprap and open source — reprap,. URL: [https://reprap.org/mediawiki/index.php?title=RepRap\\_and\\_Open\\_Source&oldid=152640](https://reprap.org/mediawiki/index.php?title=RepRap_and_Open_Source&oldid=152640). [Online; accessed 19-February-2019 ].
- [54] Shang, J., Tian, X., Luo, M., Zhu, W., Li, D., Qin, Y., Shan, Z., 2020. Controllable inter-line bonding performance and fracture patterns of continuous fiber reinforced composites by sinusoidal-path 3d printing. *Composites Science and Technology* 192, 108096. doi:10.1016/j.compscitech.2020.108096.
- [55] Silva, M.R., Pereira, A.M., Alves, N., Mateus, G., Mateus, A., Malça, C., 2019. Development of an additive manufacturing system for the deposition of thermoplastics impregnated with carbon fibers. *Journal of Manufacturing and Materials Processing* 3, 35. doi:10.3390/jmmp3020035.
- [56] Stepashkin, A., Chukov, D., Senatov, F., Salimon, A., Korsunsky, A., Kaloshkin, S., 2018. 3d-printed peek-carbon fiber (cf) composites: Structure and thermal properties. *Composites Science and Technology* 164, 319–326.
- [57] Tan, L.J., Zhu, W., Zhou, K., 2020. Recent progress on polymer materials for additive manufacturing. *Advanced Functional Materials* 30, 2003062. doi:10.1002/adfm.202003062.
- [58] Tekinalp, H.L., Kunc, V., Velez-Garcia, G.M., Duty, C.E., Love, L.J., Naskar, A.K., Blue, C.A., Ozcan, S., 2014. Highly oriented carbon fiber-polymer composites via additive manufacturing. *Composites Science and Technology* 105, 144–150.
- [59] Tian, X., Liu, T., Wang, Q., Dilmurat, A., Li, D., Ziegmann, G., 2017. Recycling and remanufacturing of 3D printed continuous carbon fiber reinforced PLA composites. *Journal of Cleaner Production* 142, 1609 – 1618. URL: <http://www.sciencedirect.com/science/article/pii/S0959652616320017>, doi:<https://doi.org/10.1016/j.jclepro.2016.11.139>.
- [60] Tian, X., Liu, T., Yang, C., Wang, Q., Li, D., 2016. Interface and performance of 3D printed continuous carbon fiber reinforced PLA composites. *Composites Part A: Applied Science and Manufacturing* 88, 198 – 205. URL: <http://www.sciencedirect.com/science/article/pii/S1359835X16301695>, doi:<https://doi.org/10.1016/j.compositesa.2016.05.032>.
- [61] Toray, . Toray vetex® tc910 pa6 carbon fiber reinforced pa6 data sheet. URL: [https://www.toraytac.com/media/694245aa-3765-43b4-a2cd-8cf76e4aee5/B3nNYQ/TAC/Documents/Data\\_sheets/Thermoplastic/UD%20tapes,%20prepregs%20and%20laminates/Toray-Cetex-TC910\\_PA6\\_PDS.pdf](https://www.toraytac.com/media/694245aa-3765-43b4-a2cd-8cf76e4aee5/B3nNYQ/TAC/Documents/Data_sheets/Thermoplastic/UD%20tapes,%20prepregs%20and%20laminates/Toray-Cetex-TC910_PA6_PDS.pdf).
- [62] TORAY, . Torayca® t300 carbon fibers data sheet. URL: [https://www.toraycma.com/file\\_viewer.php?id=4462](https://www.toraycma.com/file_viewer.php?id=4462).
- [63] Tse, L., Kapila, S., Barton, K., 2016. Contoured 3d printing of fiber reinforced polymers, in: *Proceedings of the 26th Annual International Solid Freeform Fabrication Symposium*.
- [64] Van De Steene, W., Verstockt, J., Degrieck, J., Ragaert, K., Cardon, L., 2018. An evaluation of three different techniques for melt impregnation of glass fiber bundles with polyamide 12. *Polymer Engineering & Science* 58, 601–608.
- [65] Van Der Klift, F., Koga, Y., Todoroki, A., Ueda, M., Hirano, Y., Matsuzaki, R., 2015. 3d printing of continuous carbon fibre reinforced thermo-plastic (cfrtp) tensile test specimens. *Open Journal of Composite Materials* 6, 18.
- [66] Vaneker, T., 2017. Material extrusion of continuous fiber reinforced plastics using commingled yarn. *Procedia CIRP* 66, 317–322.
- [67] Yamawaki, M., Kouno, Y., 2018. Fabrication and mechanical characterization of continuous carbon fiber-reinforced thermoplastic using a preform by three-dimensional printing and via hot-press molding. *Advanced Composite Materials* 27, 209–219. doi:10.1080/09243046.2017.1368840, arXiv:<https://doi.org/10.1080/09243046.2017.1368840>.
- [68] Yang, C., Tian, X., Liu, T., Cao, Y., Li, D., 2017. 3d printing for continuous fiber reinforced thermoplastic composites: mechanism and

performance. *Rapid Prototyping Journal* 23, 209–215.

[69] Zhuo, P., Li, S., Ashcroft, I., Jones, A., Pu, J., 2017. 3d printing of continuous fibre reinforced thermoplastic composites, in: *Proceedings of the 21st International Conference on Composite Materials, ICCM21*, ID, Xi'an, China.

[70] Zhuo, P., Li, S., Ashcroft, I.A., Jones, A.I., 2021. Material extrusion additive manufacturing of continuous fibre reinforced polymer matrix composites: A review and outlook. *Composites Part B: Engineering* , 109143doi:10.1016/j.compositesb.2021.109143.

Continuous fibre composite 3D printing with pultruded carbon/PA6 commingled fibres

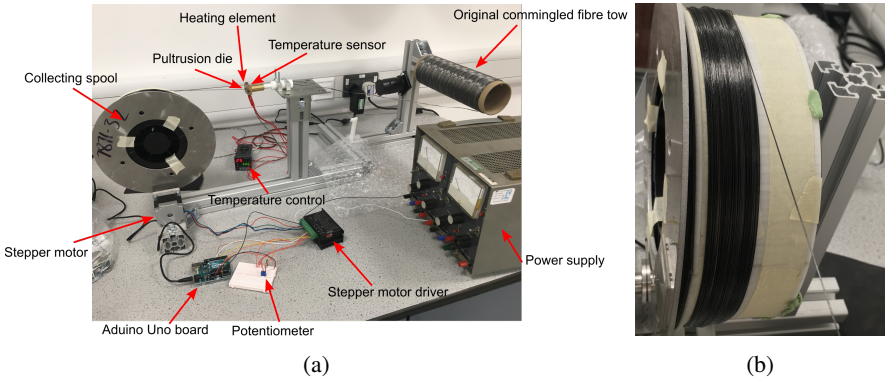


Figure 1: (a) Commingled fibre pultrusion apparatus; (b) Pultruded commingled fibre filament.

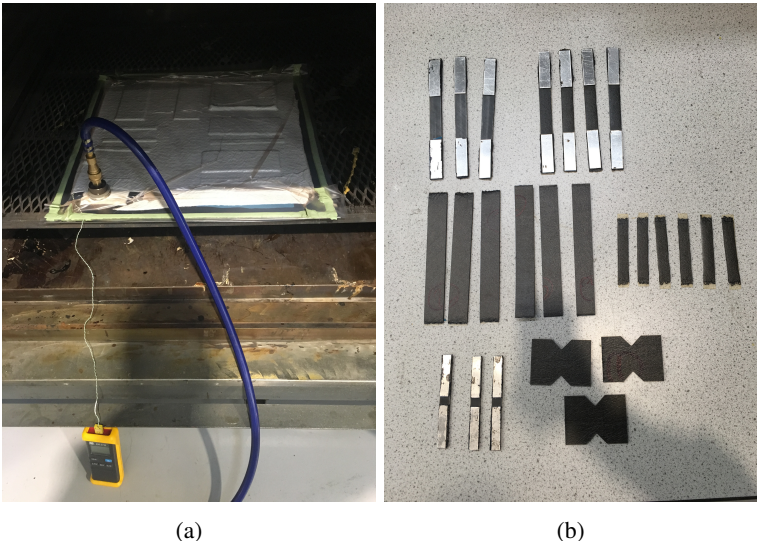


Figure 2: (a) Specimens undergoing post-processing in an oven; (b) Specimens after post-processing.



Figure 3: Optical microscope picture of the original carbon/PA6 commingled fibre tow.

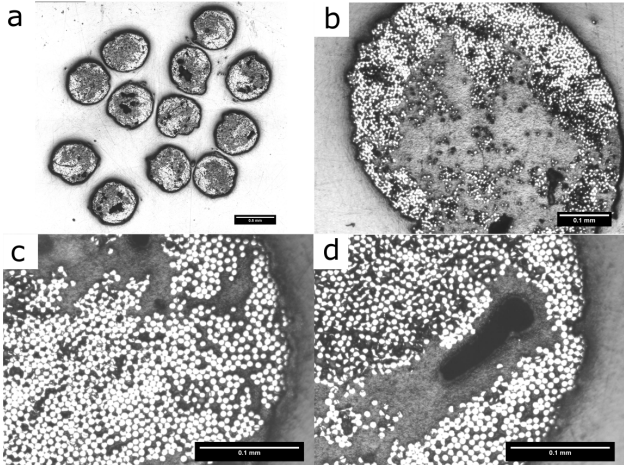


Figure 4: Pultruded filament cross-section optical microscope pictures.

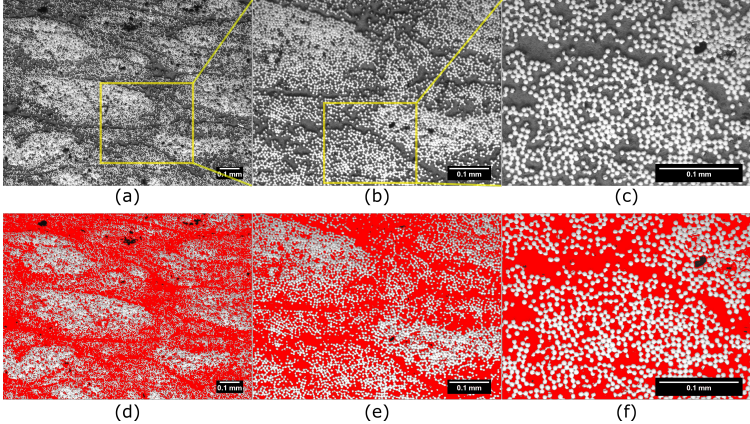


Figure 5: Fibre volume content and void content estimation on the printed sample of region 1 using optical microscopy and ImageJ software: (a) 25 times magnification; (b) 50 times magnification; (c) 100 times magnification. In subfigures (d)-(f), white is carbon fibre, red is matrix region, black is void content.

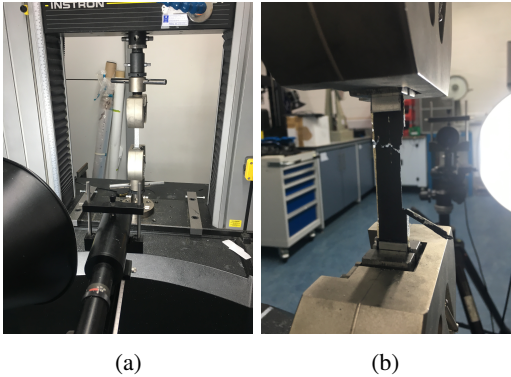
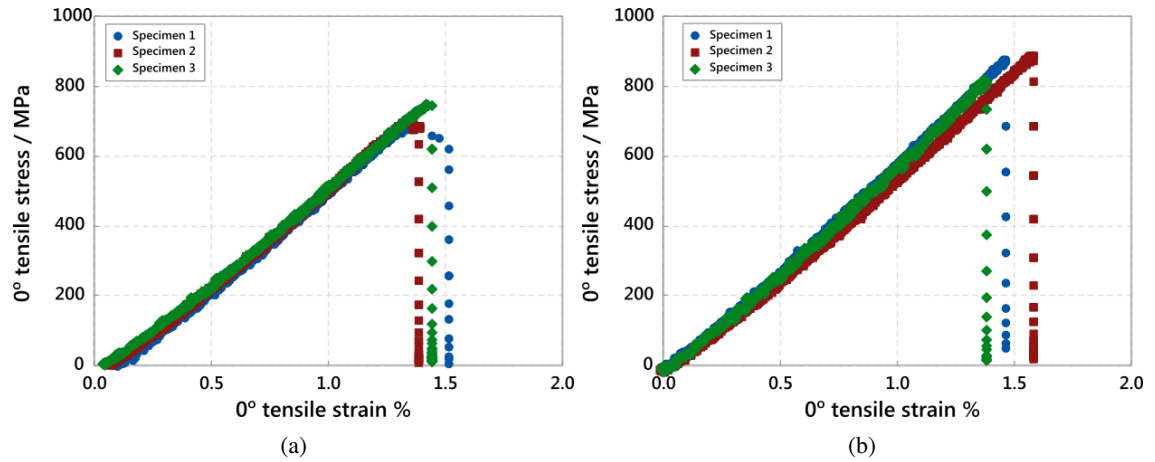
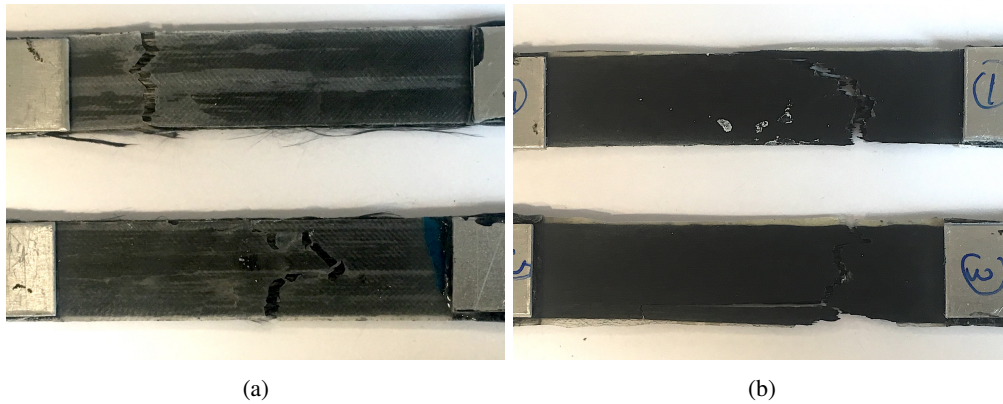


Figure 6: (a) 0° tensile test setup (b) 0° tensile test failed specimen.



**Figure 7:** Fractured specimens : (a) Stress and strain curves of the continuous fibre 3D printed 0° tensile test specimens without post-processing; (b) Stress and strain curves of the continuous fibre 3D printed 0° tensile test specimens with post-processing.



**Figure 8:** Fractured specimens : (a) without post-processing; (b) with post-processing.

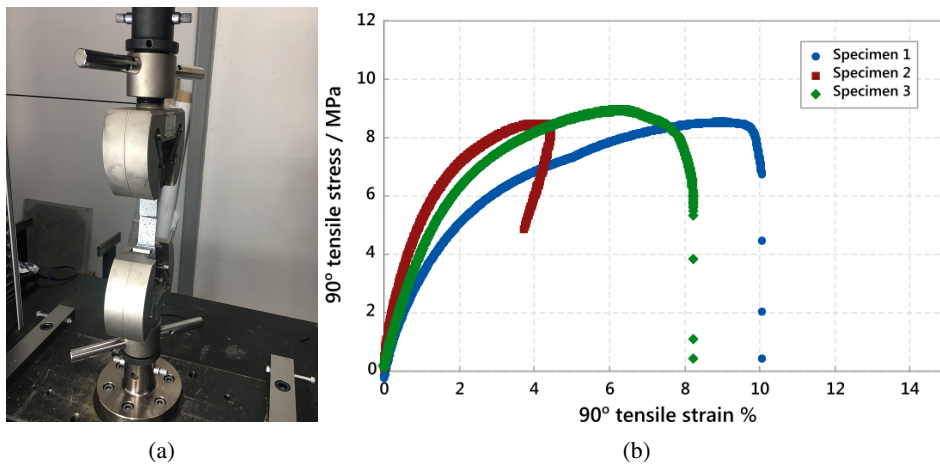


**Figure 9:** (a) 90° tensile test failed specimen; (b) Stress and strain curves of the continuous fibre 3D printed 90° tensile test specimens.

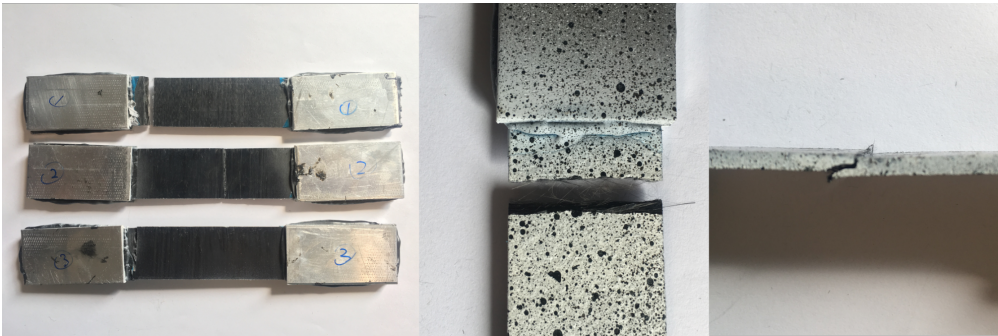


Figure 10: 90° tensile test fractured specimens.

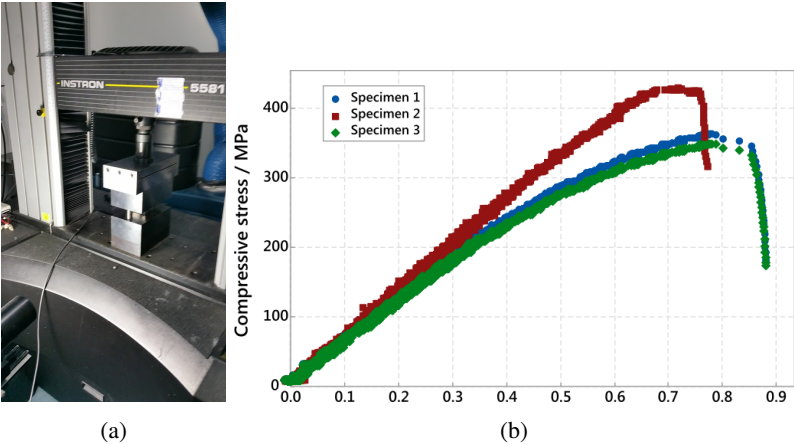


Figure 11: (a) compressive test setup; (b) In-plane compressive test stress and strain curves.

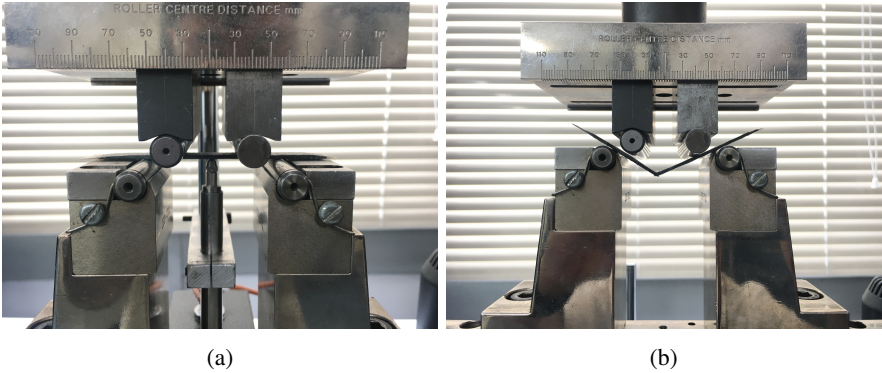


Figure 12: (a) 4-point bending test set-up for modulus measurement; (b) failed specimen in 4-point bending test.

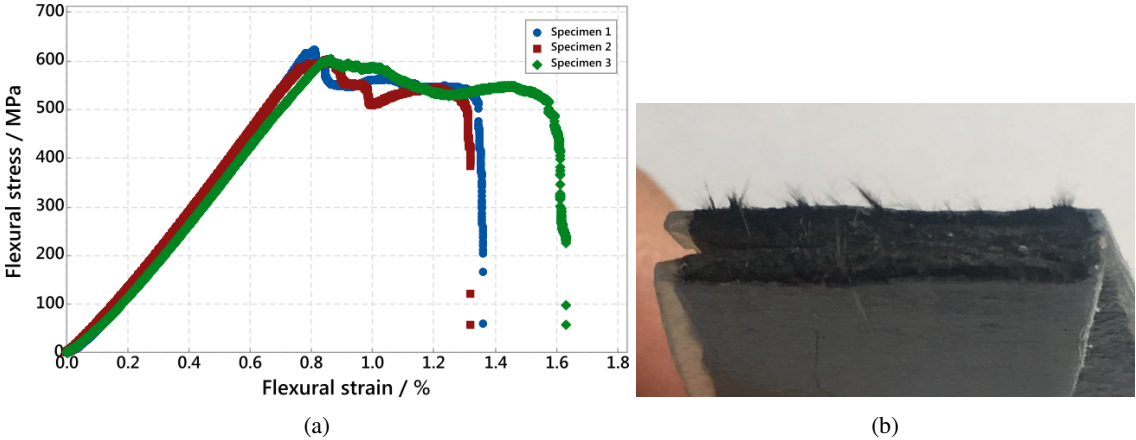


Figure 13: (a) 4-point bending test stress and strain curves; (b) 4-point bending test fractured specimens.

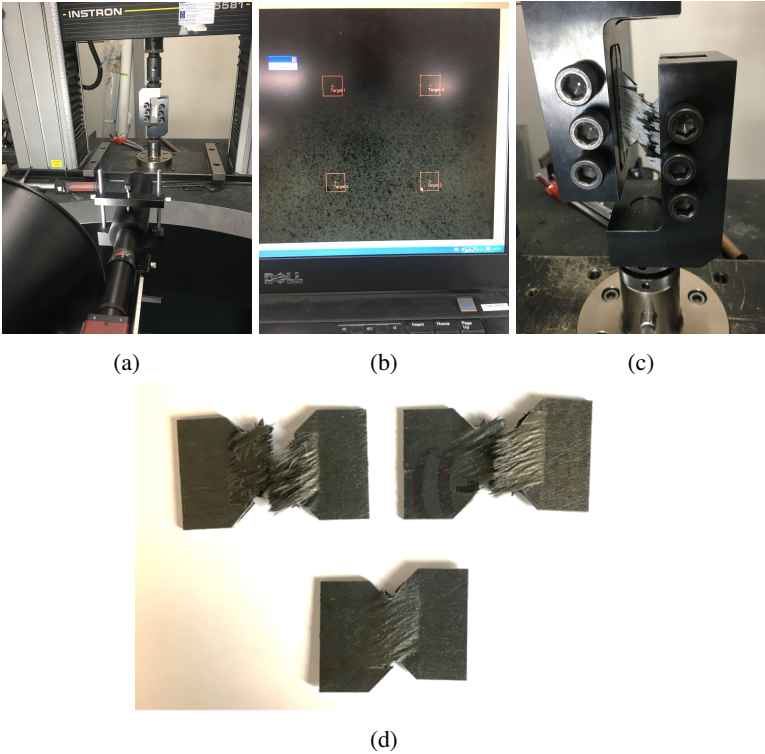


Figure 14: (a) v-notched rail shear test set-up; (b) v-notch rail shear test strain measurement target points; (c) failed specimen in v-notched rail shear test fixture; (d) v-notched rail shear test failed specimens.

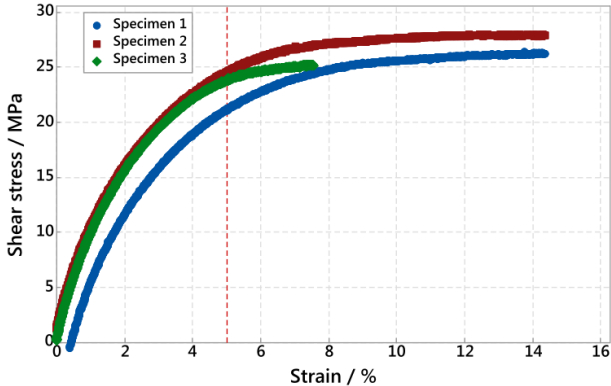


Figure 15: Stress and strain curves of the V-notch shear test specimens.

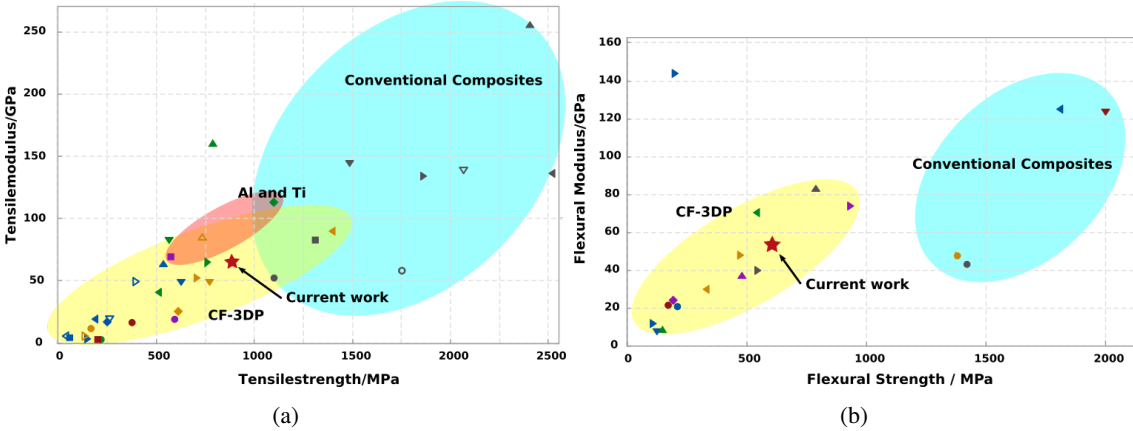


Figure 16: (a) Tensile strength vs. Tensile modulus of CF-3DP composites, conventional composites, aluminium and titanium; (b) Flexural strength vs. Tensile modulus of CF-3DP composites and conventional composites.

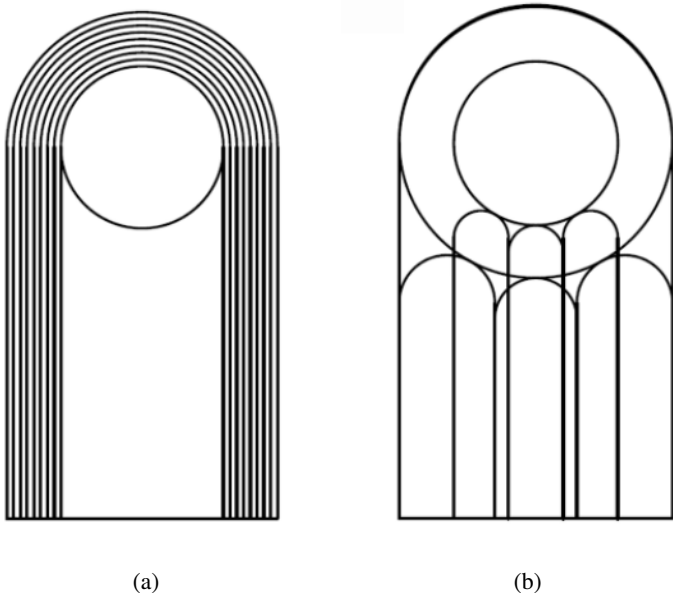


Figure 17: (a) preliminary fibre path design for a lug shape structure in tensile load case; (b) preliminary fibre path design for a lug shape structure in compressive load case.

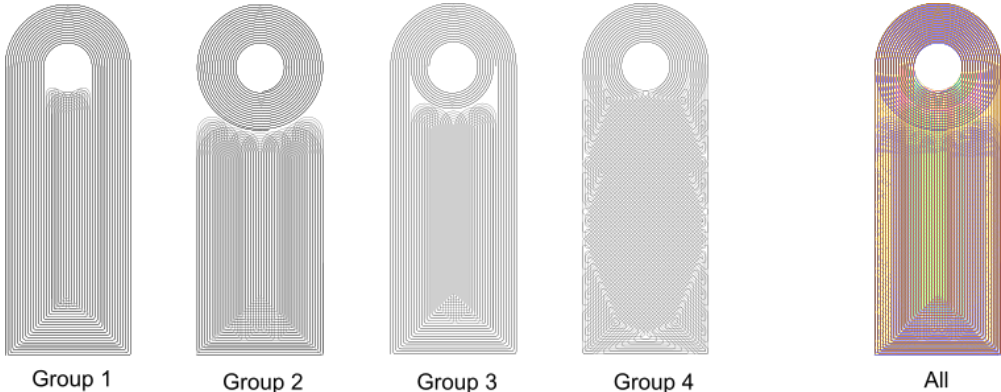
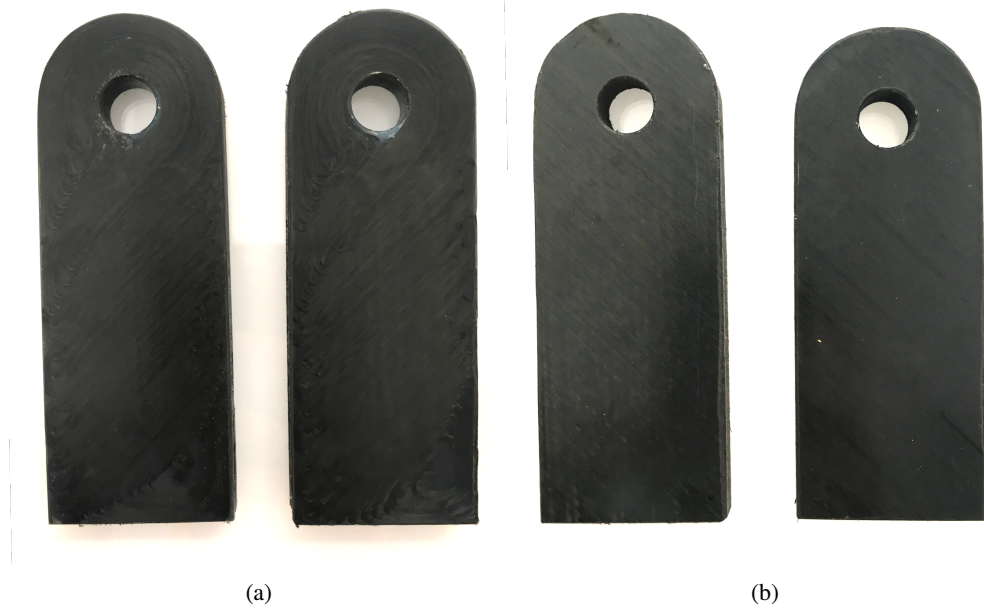


Figure 18: Overlap view of fibre patterns groups and all patterns.



**Figure 19:** (a) Lug shape samples with curvilinear fibre design after trimming; (b) Lug shape samples with quasi-isotropic layup after machining.

**Table 1**

Pultruded commingled fibre diameter and fibre volume fraction measurement

	Fibre number (n)	Fibre diameter (D)	Fibre volume	Volume fraction
Carbon fibre	3000	7 $\mu$ m	0.115mm <sup>2</sup>	55%
PA6 fibre	73	40 $\mu$ m	0.092mm <sup>2</sup>	45%
Pultruded filament	1	0.51mm	0.207mm <sup>2</sup>	100%

**Table 2**

Test standards and dimensions of the specimens.

Test methods	Length / mm	Width / mm	Thickness / mm	Endtab length / mm	Endtab thickness	Test standard
0° tensile	180	15	1	50	1	ASTM D3039
90° tensile	180	25	2	50	1	ASTM D3039
compressive	110	10	2	50	1	ASTM D410
4-point bending	77	13	2	-	-	ASTM D7264
V-notched rail shear	76	56	2.5	-	-	ASTM D7078

**Table 3**

Printing process parameters.

Printing temperature	Print speed	Layer height	Raster distance	Post-processing temperature	Post-processing time
260°C	400mm/min	0.3	0.8	220°C	15min

**Table 4**

Fibre volume content and void content of continuous fibre 3D printed sample.

	Magnification	Fibre volume content %	Matrix volume content %	Void content %
Printed sample	25	45.25	54.11	0.64
	50	45.42	54.05	0.53
	100	45.81	53.78	0.61
Pultruded fibre filament	25	47.74	46.90	5.36

**Table 5**  
Mechanical testing results.

	Specimen type	1	2	3	Average	Standard Deviation
0° tensile Strength / MPa	Without Post-processing	687	704	747	713	31.3
0° tensile Modulus / GPa		59.2	56.1	56.8	57.4	1.65
Specimen Thickness / mm		1.12	1.09	1.10	1.10	0.0153
0° tensile Strength / MPa	With Post-processing	875	888	816	859	38.1
0° tensile Modulus / GPa		62.0	57.4	63.8	61.1	3.31
Specimen Thickness / mm		1.06	1.03	1.02	1.04	0.0208
90° tensile Strength / MPa	With Post-processing	8.54	8.48	8.95	8.66	0.256
90° tensile Modulus / GPa		0.372	0.430	0.342	0.381	0.0447
Specimen Thickness / mm		2.23	2.16	2.11	2.17	0.0603
Compressive Strength / MPa	With Post-processing	348	412	342	367	42.7
Compressive Modulus / GPa		61.4	70.9	64.9	65.8	4.81
specimen Thickness / mm		2.03	2.08	2.07	2.06	0.0265
Flexural Strength / MPa	With Post-processing	576	622	602	600	23.4
Flexural Modulus / GPa		55.9	53.9	53.5	54.4	1.31
specimen Thickness / mm		1.93	1.97	1.92	1.94	0.0265
Shear Strength / MPa	With Post-processing	21.8	24.5	23.8	23.4	1.43
Shear Modulus / GPa		1.01	1.06	1.10	1.05	0.0451
specimen Thickness / mm		3.11	3.12	3.07	3.10	0.0265